Published in final edited form as:
Biomaterials. 2014 January ; 35(1): . doi:10.1016/j.biomaterials.2013.09.091.

Avidin as a Model for Charge Driven Transport into Cartilage and Drug Delivery for treating Early Stage Post-traumatic Osteoarthritis

Ambika G. Bajpayee[1], **Cliff R. Wong**[2], **Moungi G. Bawendi**[2], **Eliot H. Frank**[3], and **Alan J. Grodzinsky**[1,3,4]

[1]Department of Mechanical Engineering, MIT, 77 Massachusetts Avenue, Cambridge, MA 02139, USA

[2]Department of Chemistry, MIT, 77 Massachusetts Avenue, Cambridge, MA 02139, USA

[3]Center for Biomedical Engineering, MIT, 77 Massachusetts Avenue, Cambridge, MA 02139, USA

[4]Departments of Biological Engineering and Electrical Engineering and Computer Science, MIT, 77 Massachusetts Avenue, Cambridge, MA 02139, USA

Abstract

Local drug delivery into cartilage remains a challenge due to its dense extracellular matrix of negatively charged proteoglycans enmeshed within a collagen fibril network. The high negative fixed charge density of cartilage offers the unique opportunity to utilize electrostatic interactions to augment transport, binding and retention of drug carriers. With the goal of developing particle-based drug delivery mechanisms for treating post-traumatic osteoarthritis, our objectives were, first, to determine the size range of a variety of solutes that could penetrate and diffuse through normal cartilage and enzymatically treated cartilage to mimic early stages of OA, and second, to investigate the effects of electrostatic interactions on particle partitioning, uptake and binding within cartilage using the highly positively charged protein, Avidin, as a model. Results showed that solutes having a hydrodynamic diameter ≤ 10 nm can penetrate into the full thickness of cartilage explants while larger sized solutes were trapped in the tissue's superficial zone. Avidin had a 400-fold higher uptake than its neutral same-sized counterpart, NeutrAvidin, and >90% of the absorbed Avidin remained within cartilage explants for at least 15 days. We report reversible, weak binding (K_D ~150 μM) of Avidin to intratissue sites in cartilage. The large effective binding site density (N_T ~ 2920 μM) within cartilage matrix facilitates Avidin's retention, making its structure suitable for particle based drug delivery into cartilage.

Keywords

Cartilage; Post-traumatic Osteoarthritis; Transport; Size; Charge; Electrokinetics; Avidin; Drug Delivery

Corresponding Author: Alan J. Grodzinsky, MIT Room NE47-377, 500 Technology Square, Cambridge, MA, USA, 617-253-4969 (Phone), 617-258-5239 (FAX), alg@mit.edu.

1. Introduction

Osteoarthritis (OA) is a complex debilitating disease that affects millions of people worldwide, causing loss of productivity, quality of life, and loss of joint function. It is now accepted that OA is a disease of the entire joint, eventually affecting all joints tissues including cartilage, bone, ligaments, menisci, the joint capsule, synovial membrane, muscles and neural tissue [1,2]. Distinct subtypes of OA are associated with the varying risk factors that mediate OA initiation and progression; these risk factors include improper joint mechanics, gender, age, obesity, genetic and metabolic factors, and acute joint injury leading to post-traumatic OA (PTOA) [3, 4]. PTOA accounts for 12% of the total OA population [5]. Approximately 50–80% of young active individuals who suffer traumatic joint injuries (e.g., rupture of the anterior cruciate ligament or meniscus) progress to PTOA within 10–20 years [6, 7]. Following acute joint injury, there is an immediate increase in synovial fluid levels of inflammatory cytokines (e.g., IL-1, IL-6, TNFα) which can diffuse into cartilage and rapidly initiate proteolysis and loss of cartilage matrix [8, 9]. By the time of clinical (radiographic) diagnosis, irreversible changes to cartilage and other joint tissues have often occurred [6]. Since the cause and time of the initial trauma is known, there exists a unique opportunity for early drug intervention to prevent further degeneration of cartilage and other tissues, and to reverse the course of PTOA by inducing repair [6].

While there are disease-modifying anti-rheumatic drugs (DMARDS) for rheumatoid arthritis and several related rheumatic diseases (such as the TNFα-blockers [10]), no efficacious disease-modifying osteoarthritis drugs (DMOADS) are yet available, i.e., drugs which alter or halt the progression of OA [1,11,12]. Current therapies provide only short term relief of pain and inflammation (e.g., analgesics, hyaluronic acid lubricants, etc.), but afford no protection against further degeneration of cartilage, the hallmark of end-stage OA [3], leading to the need for joint replacement. Several anti-catabolic and pro-anabolic drugs have been identified as potentially useful to reverse or prevent PTOA-associated breakdown of cartilage, including anti-catabolic glucocorticoids (e.g., dexamethasone) and pro-anabolic growth factors (e.g., IGF-1, FGF-18, and BMP-7) [13–16]. Consistent with the concept that generalized OA involves the whole joint, DMOAD development and associated clinical trials are now targeting cartilage breakdown (e.g., protease and cytokine inhibitors), bone remodeling (e.g., bisphosphonates, BMP-7, calcitonin), and synovial and inflammatory mediators (e.g., cytokine blockers) [11]. However, no drug candidates have yet passed the safety/efficacy hurdle, and systemic drug side-effects have been a major safety concern causing several trial failures to-date [12]. Thus, it is important to develop appropriate drug delivery methods to administer potentially efficacious drugs or drug combinations directly to selected target tissues, such as cartilage thereby eliminating any systemic adverse effects [17].

It is also essential to enable rapid drug penetration throughout cartilage and to facilitate retention and sustained delivery to specific cell and matrix targets within the tissue. Recent research has focused on drug-encapsulating polymeric particles for use by intra-articular injection [17, 18]. Their effectiveness depends on their ability to enter the dense extracellular matrix (ECM) of cartilage and to be retained over time. A variety of particles have been explored in vitro and in vivo [19–23] but the effects of particle size and surface morphology on their penetration, binding and retention within cartilage are less well understood [24]. The relative utility of 15 nm micelles vs. 138 nm liposomes was recently reported, showing the need to further differentiate between size and structure [25].

The present study focuses on developing particle based drug delivery mechanisms for treating PTOA by investigating the effects of particle size and surface charge on transport, binding and retention within cartilage. Cartilage is an avascular tissue having a dense ECM

of collagen fibrils, aggrecan proteoglycans containing highly negatively charged glycosaminoglycan (GAG) chains, and many other extracellular proteins which are continuously synthesized by the low density of chondrocytes. The type II collagen network mesh size is 60–200 nm [26], while the distance between GAG chains on aggrecan is only 2–4 nm apart from each other [27]. Aggrecan density increases with depth into cartilage from the surface (superficial) zone and restricts the ability of solutes to penetrate and diffuse within cartilage [28]. Maroudas et al. [28, 29] showed that serum albumin (MW 69 kDa, diameter~7 nm, pI~ 4.7) was sterically hindered in normal human cartilage, with a partition coefficient less than 0.05, which increased in OA cartilage. Immunoglobulin (IgG) antibodies (MW~160 kDa) were sterically excluded by cartilage ECM. However, Fab antibody fragments (e.g., an anti-IL-6 Fab, 48 kDa [30]) can diffuse into bovine and human cartilage over 3 days. Fab uptake was higher in the superficial compared to deeper zones, suggesting that transport is dependent on the aggrecan content. These reports suggest the need for investigating nano-sized particles for delivery into cartilage.

While transport of solutes is size and shape dependent, binding within cartilage ECM is also modulated by particle surface properties including charge. The high negative fixed charge density of cartilage is known to regulate Donnan partitioning and binding of proteins, growth factors and other macromolecules. For example, negatively charged albumin partitions downward [28], while the positively charged growth factor IGF-1 (pI 8.5) partitions upward into cartilage [31]. Here, we investigate Avidin, a globular and highly glycosylated protein, as an example of a structure that due to its size (MW 66 kDa, diameter ~7 nm) and high positive charge (pI 10.5) may offer unique advantages for rapid uptake and binding within the tissue. Avidin has been previously investigated for targeted delivery into tumors [32]; results showed enhanced tissue and cellular uptake and binding due, in part, to electrostatic interactions.

With the goal of developing particle-based drug delivery mechanisms for treating PTOA, the objectives of this study were (1) to determine the size range of a variety of solutes that could penetrate and diffuse through normal and enzymatically treated cartilage to mimic early stages of OA, and (2) to investigate the effects of electrostatic interactions on solute uptake, partitioning and binding within cartilage by using the highly positively charged protein, Avidin.

2. Materials and methods

In a series of transport studies, cartilage disks were incubated in medium containing a range of fluorescently tagged solutes of varying size and charge. Cross-sections of the cartilage were then imaged using confocal microscopy to determine the depth of penetration and the spatial distribution of each solute type within the tissue. In separate experiments to obtain a measure of total solute uptake, cartilage disks were equilibrated in solutions of selected solutes and then desorbed into phosphate buffered saline (PBS) baths. The measured fluorescence in the absorption and desorption baths were used to quantify the equilibrium uptake ratio, partition coefficient, and equilibrium binding properties of these solutes within the tissue. Additional studies of non-equilibrium transport through cartilage disks enabled estimation of the effective diffusivity of selected solutes within cartilage.

2.1. Bovine cartilage harvest and culture

Cartilage disks were harvested from the femoropatellar grooves of 1–2 week old bovine calf knee joints (obtained from Research 87, Hopkinton, MA) as described previously [33]. Briefly, cylindrical cartilage disks (3 mm or 6 mm diameter) were cored using a dermal punch and then sliced to obtain the top 1mm of cartilage with intact superficial zone. Cartilage disks for all treatment groups were matched for depth and location along the joint

surface. The disks were then pre-equilibrated in PBS (without Ca^{2+}/Mg^{2+}) supplemented with protease inhibitors (Complete Protease Cocktail tablet in 50 mL PBS, Roche Applied Science, IN) in a 37°C, 5% CO_2 incubator for 24–48h.

2.2. Solutes Types

2.2.1 Size exclusion studies—We used solutes having a wide range of sizes from ~0.9 nm to 15 nm diameter: (i) fluorescein isothiocyanate (FITC, 389.3 Da, diam ~0.9 nm), (ii) FITC-dextran (8 kDa, hydrodynamic diameter 4.3 nm), (iii) FITC-dextran (40 kDa, diameter ~10 nm (all from Sigma Aldrich, MO); (iv) FITC-conjugated NeutrAvidin, an electrically neutral globular protein at pH 7 (60 kDa, diameter ~7 nm; Invitrogen, CA) and (v) Cd-Se Quantum Dots 15 nm in diameter (Red, synthesized at MIT [34]).

2.2.2 Binding/Retention studies—Effects of electrostatic interactions on solute transport, uptake and binding were investigated by using (i) FITC-conjugated and non-labeled Avidin (pI 10.5, 66 kDa, diameter ~7 nm, Invitrogen, CA), the positively charged counterpart of NeutrAvidin, and (ii) amine functionalized 15 nm diameter Cd-Se quantum dots (QDs) (Qdot ®565, Green, Invitrogen, CA, USA). FITC-dextran (8kDa) was dialyzed using 1 kDa MW cut off dialysis tube (Float-A-Lyzer G2, SpectrumLabs Inc., CA) and all other solutes were dialyzed using 3 kDa cutoff MW centrifugal filter (Amicon Ultra-4, Millipore Corp, MA) to determine the amount of free FITC; the fluorescence readings of these solutions after dialysis indicated negligible amounts of free FITC. The solute types with their physical properties are listed in Table 1.

2.3. Transport Configuration for Confocal Microscopy Imaging

A special poly(methyl methacrylate) (PMMA) transport chamber was designed to study one-way diffusion of solutes entering into cartilage from the tissue's superficial zone (SZ) (i.e., transport in the X direction in Fig. 1). The chamber walls were treated with casein to block non-specific binding of solutes to PMMA surfaces. Pre-equilibrated cartilage disks (6 mm diameter, 1 mm thick) were first cut in half, and the half-disk specimens were placed within holding slots machined into the chamber (Fig 1A). The upstream chamber side facing the superficial zone was filled with 45 μl of a known concentration of solute in 1X-PBS solution supplemented with protease inhibitors (Roche Applied Science, IN); the downstream chamber side was filled with 45 μl of 1X-PBS containing protease inhibitors alone. The chamber was then placed in a petri dish containing DI water, covered (to minimize evaporation), and placed on a slow-speed rocker inside an incubator at 37°C to minimize stagnant layers at cartilage surfaces.

After 24–96 h, the cartilage half-disks were removed from the bath, gently rinsed in 1X PBS, and surface fluid along with any non-absorbed solutes were gently removed with Kimwipes. Using a scalpel, a slice (100–200 μm thick) was then cut from the center of each disk (Fig. 1B). The middle region of the slice (shown by the dotted boundary) was imaged in the X-Y plane using a confocal microscope (Nikon TE2000-U) at 10X magnification to identify the penetration and X-directed solute concentration profile within the tissue. Appropriate optical filters were chosen to eliminate auto-fluorescence of cartilage at the settings used for imaging. For desorption studies, the solute solution was removed from the chamber of Fig. 1 and replaced with 1X or 10X PBS containing protease inhibitors. To ensure proper image comparison, solute concentrations were chosen such that the FITC concentration in each solution was identical, thereby giving equal fluorescence intensities. Nominal concentrations for the absorption baths were 2.5 μM (FITC), 125 μM (FITC-dextran, 8 kDa), 25 μM (FITC-dextran, 40kDa), 18 μM (Avidin), and 30 μM (NeutrAvidin). 100 μM (FITC-Dextran, 40 kDa) was also used for a separate 24–96 h transport study (Fig.

2D–F). The concentrations for the two types of QD solutions were chosen such that they exhibited equal fluorescence intensity.

2.4. Quantitative analysis of solute uptake into cartilage

2.4.1 Quantum Dot Uptake using Induced Coupled Plasma Measurement—The total uptake of QDs into cartilage half disks was measured via quantification of the amount of cadmium (^{111}Cd) present in the tissue and the absorption/desorption baths that were collected immediately after each QD uptake experiment. (Cd is present in the core of QDs). Inductively coupled optical-emission spectrometry (ICP-OES) was performed using a Horiba Jobin Yvon Activa ICP OES (Horiba Scientific, NJ) to quantify the amounts of ^{111}Cd using a previously published method [35]. The sum of final amounts of Cd in the bath and the cartilage half disks corresponded to the initial amount of Cd in the starting 45 μl of QD-PBS upstream solution. The Cd amounts were converted into QD concentrations using calibration plots made for each QD studied. The background amount of Cd in fresh, untreated cartilage was measured to be zero.

2.4.2 Equilibrium uptake of Avidin and NeutrAvidin—3 mm diameter, 1 mm thick cartilage explants were incubated for specific times in 300 μl of known concentration (3μM) of FITC-Avidin and FITC-NeutrAvidin, supplemented with protease inhibitors at 37°C in a 96 well plate format. After removal from the absorption baths, the disks were rinsed, gently wiped and then incubated in 1X or 10X PBS supplemented with protease inhibitors for 24 h or longer as specified. At the end of the experiment, the surfaces of each disk were quickly blotted with Kimwipes and the wet weight was measured. The disks were then lyophilized and the dry weight was measured; the water weight was calculated from the tissue wet and dry weights. The fluorescence signal in the absorption and desorption baths was quantified using a plate reader (1400 Wallace Victor, PerkinElmer, MA); the solute content inside the cartilage disk was determined from the difference between the fluorescence reading of the absorption/desorption baths before and after incubation. In establishing standard curves, the fluorescence intensities and solute concentrations for both FITC-Avidin and FITC-NeutrAvidin were found to be linear with bath concentration. The solute uptake ratio was calculated as the concentration of the FITC-solute in the cartilage (per intra-tissue water weight) normalized to the concentration of FITC-solute in the equilibration bath.

2.5. Effect of sGAG Depletion on solute uptake

To understand the effects of the negatively charged glycosaminoglycan (GAG) chains within cartilage matrix on solute uptake and binding, groups of cartilage disks (3 mm diameter, 1 mm thick) were treated with either chondroitinase-ABC (Sigma Aldrich, MO, USA), or trypsin (Invitrogen, CA). Chondroitinase-ABC digests and removes GAG chains (predominantly the chondroitin sulfate GAG chains of the highly abundant aggrecan proteoglycans in cartilage) while the protease, trypsin, cleaves the core proteins of aggrecan and other GAG-containing proteoglycans and glycoproteins. However, both treatments leave cartilage's collagen network intact [36]. The dimethyl-methylene blue (DMMB) dye binding assay [37] was used to quantify the content of sulfated GAG (sGAG) remaining in the disks after enzyme treatment as well as that lost to the medium as previously described [14], and the percentage of GAG removed by specific enzyme treatments was thereby calculated. For one series of experiments, a 24 h chondroitinase-ABC treatment (0.1U/ml in 0.15 *M* NaCl, 0.05 M Na phosphate, pH 7.2 for 24 h at 37°C) was used, resulting in 38.6% (~40%) depletion of sGAG, primarily from the outer tissue surfaces, which mimics the initial GAG loss caused by traumatic joint injury in vivo [38] and in models of cartilage injury in vitro [39]. A second group of disks was treated with trypsin (1 mg/ml, in 0.15 *M* NaCl, 0.05 M Na phosphate, pH 7.2 for 24 h at 37°C). Previous studies showed that treatment of similar bovine calf cartilage disks with 1 mg/ml trypsin caused nearly complete loss of measureable

sGAG by 24 h [40]. After enzyme treatments, the disks were washed three times in fresh PBS. Uptake experiments were then conducted using solute-PBS solutions containing protease inhibitors to minimize any additional protease activity. The transport and binding properties were then compared with that in the normal cartilage.

2.6. Transport Measurements for Effective Diffusivity

Real-time measurement of diffusive transport of Avidin and NeutrAvidin through young bovine cartilage disks (with intact superficial zone) was measured using a diffusion chamber consisting of two compartments as described previously [31]. Groups of three cartilage disks (6 mm diameter, 400 μm thick) were clamped by O-rings between the two compartments of the diffusion chamber (with total exposed tissue area for transport of 0.28 cm^2/disk), such that solute transport from the upstream compartment into and across the cartilage disks, simultaneously, could occur only from the superficial zone of the cartilage (schematic shown in the inset of Fig. 7). The compartments were treated with casein to prevent non-specific adsorption of solutes to the chamber surfaces. Each compartment was then filled with 25 mL of 0.15 M NaCl with protease inhibitors and maintained at 20 °C. At starting time t = 0, FITC tagged Avidin or NeutrAvidin was added to the 'upstream' compartment, resulting in transport through the tissue into the downstream compartment. The baths in both compartments were magnetically stirred to minimize the effects of stagnant layers at the solution-tissue interfaces. Aliquots were taken from each chamber at different time intervals, and fluorescence was measured using a plate reader.

We note that the compartment volume of 25 mL is approximately 1,000 X larger than the volume of the cartilage plugs in the configuration of Fig. 7 (inset). As a result, the boundary solute concentration at the cartilage-solution interfaces, both upstream and downstream, remained to within ~5% of their starting (t=0) values throughout the course of these transport experiments. This configuration thereby focuses on quantitation of steady state solute flux and assessment of effective solute diffusivity within cartilage. In contrast, the transport chamber compartment volumes in the configuration of Fig. 1 are relatively smaller and closer to the volume of the cartilage disks, a configuration that more closely approximates the relative solid-fluid volumes of cartilage and adjacent synovial fluid in joints in vivo. (For example, human tibial plateau cartilage volume is ~4 mL [41], and knee joint synovial fluid volume ranges from ~1–4 mL [42]).

2.7. Statistical Analysis

Data on solute uptake and desorption (e.g., Figs. 3I–J and 5A–C) are presented as Mean ± SEM. We used the general linear mixed effects model with animal as a random variable for analysis followed with the Tukey's test for comparisons between multiple treatment conditions. Fig. 3 data are derived from 2 different animals. A total of n=3 cartilage samples per animal in each treatment condition were used. The mean represents the average of 6 samples per treatment condition, as there was no effect of animal. Figure 5 data are derived from 3 different animals for the normal cartilage condition and 1 animal for the 40% GAG depleted condition. A total of n=6 cartilage samples per animal in each treatment condition was used; the mean represents the average of 18 samples per treatment for the normal cartilage condition (since there was no effect of animal) and the average of 6 samples per treatment for the 40% GAG depleted condition. We used $p<0.05$ for statistical significance.

3. Results

3.1. Effect of solute size and molecular structure on transport into cartilage

Transport studies with FITC (389 Da, diameter ~0.9 nm) and FITC-dextran (8 kDa, diameter ~4.3 nm) showed that particles with hydrodynamic diameter < 5 nm penetrated

throughout the full thickness (1 mm) of the cartilage explant within 24 h, while a penetration gradient was still evident at 24 h for 40 kDa FITC-dextran (diameter ~10 nm) (Fig. 2A–C). The relative fluorescence intensity vs. penetration distance into cartilage is plotted below the images, illustrating size-dependent transport. 40 kDa FITC-dextran solutes (expandable polysaccharide coil) diffused into the major part of the cartilage thickness in 4 days (Fig. 2D–F), while the globular protein, NeutrAvidin (MW 60 kDa, diameter ~7 nm) penetrated approximately half the sample thickness (Fig. 2G–I). 15 nm diameter QDs were trapped in the cartilage superficial zone and penetrated only the first 40–50 μm of tissue in 24 h (Fig. 3A, 3C). The penetration depth of these QDs did not change even by 6 days (data not shown), suggesting that 15 nm diameter particles are too large to penetrate through the complex meshwork of cartilage matrix. However, trypsin treated samples allowed the 15 nm QDs to penetrate through the full thickness of the cartilage disk in 24 h (Fig 3E, 3G). DLS measurements (Malvern Zetasizer-ZS90 equipped with a He-Ne laser) showed no aggregation of QDs at 37°C over this time course.

3.2. Effect of particle surface properties on uptake, retention and binding within cartilage

Amine functionalized QDs (GREEN) did not desorb after 24 h in 1X PBS while the QDs with no functional group (RED) did (Fig. 3B, 3D). Desorption in 10X PBS significantly reduced the retention of green QDs in the cartilage disks from 64% to 0.4% of the absorbed amount in 24 h (Fig. 3J). Trypsin treated samples exhibited significantly lower retention (~40%) compared to normal cartilage (~64%) but retained similar amounts with 1X and 10X desorption (Fig 3J), suggesting charge based interactions. Matrix degradation due to trypsin treatment significantly enhanced the penetration and uptake for both types of QDs, as expected (Fig 3E, G, I).

To further explore the effects of electrostatic interactions, the transport and binding properties of Avidin (a highly positively charged globular protein) were compared to that of its neutral counterpart, NeutrAvidin. Despite their similar sizes, NeutrAvidin penetrated only half the specimen thickness in 4 days (mean uptake ~0.44) while Avidin diffused through the full thickness of the cartilage (mean uptake ~183) within 1 day, resulting in greater than 400 times higher uptake of Avidin compared to NeutrAvidin (Fig. 4A–C; 5A–B). About 50% of the absorbed NeutrAvidin diffused out of the cartilage within 1 day in 1X PBS, while 96% of the absorbed Avidin remained inside the cartilage even by 15 days (the duration of the experiment conducted) in 1X PBS (Fig. 5C). However, a significantly higher percent (~ 69%) of the absorbed Avidin diffused out of the cartilage in 10X PBS within 24 h, suggesting effects of strong electrostatic interactions (Fig. 4D–E). We hypothesized that the Avidin could be binding (reversibly) to the negatively charged GAG chains in the cartilage matrix. Depletion of 40% of the cartilage sGAG (using chondroitinase-ABC) resulted in significantly reduced uptake of Avidin over a 24 h period, from a mean value of 183 in normal cartilage to 24 in GAG-depleted tissue (Fig. 5A). This further confirmed the effects of charge interactions and showed that the negatively charged sGAG chains of cartilage matrix play a critical role in enhancing the transport, uptake and binding properties of large, positively charged globular proteins like Avidin. The uptake of NeutrAvidin, however, increased from 0.28 in the normal cartilage to 0.54 in GAG depleted cartilage by 24 h (Fig. 5B), which is most likely due to the increase in the matrix pore size resulting from 40% sGAG depletion.

3.3. Avidin uptake as a function of bath Avidin concentration

Based on the results of Fig 5, we hypothesized that Avidin could bind to sites within the cartilage. To test this hypothesis, we performed competitive binding experiments in which 3 mm diameter cartilage disks were equilibrated for 3 days in 300 μl buffer containing a fixed amount of (fluorescently labeled) FITC-Avidin (1 μM) and graded amounts of unlabeled

Avidin (0, 10, 76, 100, and 203 μM). The disks were split into half disks to reduce the time needed for equilibration, which was performed in 96 well plates at 37°C. The uptake ratio, R_U, was measured and plotted versus the total bath concentration of Avidin (labeled + unlabeled, Fig. 6), where R_U is defined as the total concentration of Avidin inside the cartilage (bound (C_B) plus free (C_F)) per intra-tissue water weight, normalized to the Avidin concentration in the equilibration bath (C_{Bath}):

$$R_U = \frac{C_B + C_F}{C_{Bath}} \quad (1)$$

Labeled and unlabeled Avidin were assumed to partition into the cartilage identically. At very low concentration of the labeled Avidin (≤ 1 μM), a high uptake of ~120 was observed. When unlabeled Avidin was added to the bath, both species (labeled and unlabeled) could compete for the same (constant) number of binding sites available in the tissue (site density N_T). As the concentration of unlabeled Avidin was increased, the uptake of labeled Avidin was observed to decrease dramatically (Fig. 6). To model the data of Fig. 6, we assumed a simple first-order, bimolecular, reversible reaction to describe binding of Avidin to a single dominant binding species within cartilage. We adopted a similar previously described theoretical model [31] used for characterizing the binding of soluble insulin like growth factor-1 (IGF-1) to IGF-binding proteins (IGF-BPs) that are uniformly enmeshed and fixed within cartilage matrix. According to this model, the equilibrium molar concentration of free solute (C_F), bound solute (C_B), intra-tissue binding site density (N_T) and the equilibrium dissociation constant (K_{EQ}) are related by the binding isotherm:

$$\frac{C_B}{C_F} = \frac{N_T}{K_{BQ} + C_F} \quad (2)$$

which is similar in form to a Langmuir adsorption isotherm. In addition, the equilibrium partition coefficient (K) of solute, Avidin, is defined as the concentration of the free solute inside the cartilage disk (per intra-tissue water weight) normalized to the concentration of solute in the bath:

$$K = \left(\frac{C_F}{C_{Bath-final}}\right)_{\text{unlabeled Avidin}} = \left(\frac{C_F}{C_{Bath-final}}\right)_{FITC-Avidin} \quad (3)$$

In these experiments, the final Avidin bath concentration in Equation (3), $C_{Bath\text{-}final}$, is generally different from the initial bath concentration, $C_{Bath\text{-}initial}$, because of the very high uptake of Avidin into cartilage. The ratio of final to initial Avidin bath concentration is defined as *f*:

$$\left(\frac{C_{Bath-final}}{C_{Bath-inital}}\right)_{FITC-Avidin} = \left(\frac{C_{Bath-final}}{C_{Bath-initial}}\right)_{unlabeled} = f$$

Then the partitioning of labeled and unlabeled Avidin into cartilage then becomes:

$$C_F = KfC_{Bath-initial} \quad (4)$$

Combining Equations 1–4 yields:

$$R_U = K\left(1+\frac{N_T}{K_{EQ}+KfC_{Bath-initial}}\right) \quad (5)$$

The theoretical curve for R_U was fit to the data of Fig. 6 (solid line) using nonlinear least squares; the best fit values for the three unknown parameters were, K = 5.9, K_{EQ} = 150.3 μM and N_T = 2920 μM. We note that the partition coefficient K is the value of in Eq. (5) in the limit of very high Avidin bath concentration (i.e., the limit in which all the binding sites are occupied by the unlabeled Avidin). Thus, K is determined by both steric hindrance and electrostatic (Donnan) interactions. (The data of Fig 6, re-plotted in the form of the binding isotherm of Eq. (2), is presented in Supplemental Section S1 for comparison.)

3.4. Characterization of non-equilibrium transport of Avidin across bovine cartilage

The transport cell arrangement shown in the inset of Fig. 7 was used to measure transient transport of Avidin and NeutrAvidin into and across cartilage disks. Fig. 7 shows real time measurements of the downstream concentration of FITC-Avidin (normalized to upstream concentration) that had diffused through a group of three cartilage explants in parallel. Extrapolation of the linear slope of concentration versus time (between t = 50 to t = 150 minutes) to the time axis gives the time lag τ_{lag} to achieve the steady state flux [43] which, for Avidin, was τ_{lag} ~ 35 min. This τ_{lag} is related to the effective diffusivity, D_{EFF}, of Avidin that characterizes the initial transport transient [43]:

$$\tau_{lag} = \frac{\delta^2}{6\,D_{EFF}} \quad (6)$$

where δ is the thickness of the cartilage disk (~400 μm). D_{EFF} for Avidin was calculated to be 3.8×10^{-7} cm^2/s. We hypothesized that this time lag and, hence, D_{EFF} could be associated in part with the effects of binding of Avidin within the cartilage. Once this binding has reached steady state, a corresponding steady state flux would be achieved, as seen in Fig 7 from t = 35 min to t = 186 min. This steady state flux is expressed in terms of the steady state diffusivity D_{SS} by:

$$\Gamma = \Phi K D_{SS}\frac{C_U - C_D}{\delta} \cong \Phi K D_{SS}\frac{C_U}{\delta} \quad (7)$$

where Φ is the tissue porosity (measured from wet and dry weights to be Φ = 0.81), K is the partition coefficient, and C_U and C_D are upstream and downstream bath concentrations, respectively. The time derivative of the normalized downstream concentration (slope) is related to the steady state flux by,

$$\frac{\partial}{\partial t}\left(\frac{C_D}{C_U}\right) = \frac{\Gamma A}{V_D C_U} \cong \frac{\Phi K D_{SS} A}{\delta V_D} \quad (8)$$

where A is the total exposed tissue area (0.84 cm^2) and V_D (25 cm^3) is the volume of the downstream bath. Using Eq. 8, the product KD_{SS} for Avidin was calculated to be 1.4×10^{-5} cm^2/s. Similarly, KD_{SS} for NeutrAvidin was calculated to be 2.3×10^{-6} cm^2/s, giving a ratio of $(KD_{SS})_{Avidin}$ to $(KD_{SS})_{NeutrAvidin}$ of ~10. Avidin and NeutrAvidin are of similar size and, hence, are expected to have similar steady state diffusivity, D_{SS}. The partition coefficient for NeutrAvidin, $K_{NeutrAvidin}$ was estimated from the data of Fig. 5B to be 0.44. Using these values, we calculated K_{Avidin} to be 4.4 and D_{SS} to be $3.2 \times 10^{-6}$$cm^2/s$.

To test whether any unbound FITC was present which could affect the measurement of the total flux and thereby the estimate of diffusivity, free FITC (MW 389.3 Da) was added at t = 186 min into the upstream bath. Almost immediately, the diffusive flux of fluorescently labeled species across the cartilage increased dramatically (Fig. 7). The diffusivity of free FITC was thereby estimated to be 2.8×10^{-5}cm^2/s, one order of magnitude higher than the steady state diffusivity (D_{SS}) calculated for Avidin, implying that there was a negligible amount of free FITC present which could affect the measurement of the flux of FITC-Avidin.

Assuming that D_{EFF} includes the effects of binding, modeled using first order, reversible bimolecular reaction kinetics, D_{EFF} can be derived in terms of D_{SS} [31]. During the initial addition of labeled Avidin, i.e., in the limit in which $C_F < K_{EQ}$, D_{EFF} is related to D_{SS} by [31]:

$$D_{EFF} \simeq D_{SS}\left(1+\frac{N_T}{K_{EQ}}\right)^{-1} \quad (9)$$

From the best fit values (section 3.2), $\left[1+\frac{N_T}{K_{EQ}}\right]=20.4$. Using $D_{EFF} \sim 3.8 \times 10^{-7}$cm^2/s (from figure 7), $D_{SS} = 7.7 \times 10^{-6}$cm^2/s, which is on the same order of magnitude as that calculated from the transport cell experiment. (See Table 2 for transport properties estimated for Avidin.)

4. Discussion

Traumatic joint injuries can result in damage to many soft and hard tissues. While joint cartilage sometimes remains undamaged, varying changes are observed, from subtle microdamage to the matrix (not visualizable by MRI or arthroscopy) up to overt fibrillation and cracks [44]. Trauma simultaneously increases the levels of inflammatory cytokines in the synovial fluid, which can predispose even undamaged cartilage to rapid chondrocyte-mediated proteolysis and loss of aggrecan and other matrix molecules within the first days/weeks post-injury [6,14,38,44,45], eventually leading to PTOA. With the need to identify drug-carrying nanoparticles that can penetrate rapidly within cartilage to provide sustained delivery of drugs to cell and matrix targets throughout the tissue, we studied a range of particle sizes and types to test their ability for rapid and sustained uptake.

We found that deep penetration into normal (undamaged) cartilage required particle diameters < 10 nm (Figs. 2–4). If injected intra-articularly, in-vivo clearance would define a practical lowest size limit [46,47]. While 15 nm diameter particles were sterically hindered and trapped in the superficial zone of normal cartilage, they could penetrate into the deeper zones of proteoglycan-depleted cartilage (Fig. 3), consistent with previous reports of solute penetration [28,29,48–51]. Such larger sized particles can be used for drug delivery if they can be functionalized to specifically bind within the superficial zone of cartilage. As these particles gradually degrade, they could release drugs which could then diffuse and/or bind within the cartilage over time. We demonstrated this approach by using amine functionalized QDs; however, the specific binding mechanism in this case is not apparent.

The high negative fixed charge density of cartilage offers the unique opportunity to utilize electrostatic interactions to augment transport, binding and retention of drug carriers. Recently, transport into cartilage explants of a small cationic peptide therapeutic was investigated (Arg-Tyr-Lys-Arg-Thr; 760 Da, net charge +3; pI = 11). The concentration of the peptide was indeed higher in cartilage due to Donnan (electrostatic) partitioning (as

would be expected), but the peptide did not bind within the cartilage and therefore rapidly diffused out [52]. Reversible binding to intra-tissue sites is necessary to maintain enhanced intra-tissue concentration for sustained local delivery, and separate experiments must be performed for any given nanoparticle to test whether electrostatic interactions can simultaneously affect non-equilibrium transport and equilibrium uptake (the latter associated with binding of solutes to matrix and/or upward Donnan partitioning of unbound solutes into intra-tissue fluid).

In this study, we report that Avidin's structure due to its size and high positive charge exemplifies distinct advantages for a particle-based drug delivery system. Avidin penetrated throughout the full thickness of cartilage explants within 24 h, while the same-sized neutral counterpart, NeutrAvidin, took four days to penetrate into half the thickness (Figs. 2,4). Avidin showed a 400 times higher equilibrium uptake compared to NeutrAvidin in normal cartilage. Additionally, Avidin was retained within cartilage for at least 15 days, while NeutrAvidin was mostly released when explants were placed in a 1X PBS desorption bath for 24 h (physiological ionic strength) (Fig. 5). When placed in high salt (10X PBS), Avidin, too, was readily desorbed due to the shielding of electrostatic interactions.

The transport of a large, positively charged molecule like Avidin through negatively charged cartilage is influenced by three phenomena (i) steric hindrance from the dense tissue ECM (characterized by D_{SS}, Eq. (7)), (ii) binding to the intra-tissue sites (characterized by D_{EFF}, which is a function of D_{SS}, N_T, and K_{EQ}, Eq. (9)), and (iii) Donnan partitioning of unbound Avidin due to electrostatic interactions (characterized by K, Eqs. (3,7)). Upon initial addition of Avidin to the bath, electrostatic interactions would result in high upward Donnan partitioning of Avidin at the solution-cartilage interface (through K). The resulting steep intra-tissue concentration gradient would greatly enhance transient transport of Avidin into the tissue compared to that of similarly sized but neutral, NeutrAvidin, as observed (Figs. 4,5). At final equilibrium, the high uptake of Avidin could be due to either intra-tissue binding and/or tissue-wide upward Donnan partitioning. To distinguish between these effects, we performed additional competitive binding experiments (Fig. 6) which suggest that Avidin binds weakly and reversibly to sites in cartilage with a K_D ~150 μM. The predicted high binding site density (N_T ~2920 μM) is consistent with the high concentration of intra-tissue GAGs, and explains Avidin's long retention time (~15 days) inside the tissue.

Further evidence of the presence of binding interactions is provided by the non-equilibrium transport experiments of Fig. 7: the measured diffusion lag time (τ_{lag}) suggests that binding slowed the initial transport of Avidin into cartilage compared with the final steady state diffusive transport across the tissue. The effective diffusivity D_{EFF} (which includes the effects of binding from Eq. (9)) was estimated from the measured τ_{lag} (Eq. (6)); D_{EFF} was an order of magnitude less than D_{SS}, the diffusivity after binding had reached steady state. Nevertheless, this weak, reversible binding did not inhibit Avidin's rapid penetration into the full depth of the explants because of the steep intra-tissue concentration gradient caused by Donnan partitioning.

Because of the importance of electrostatic interactions in the uptake and transport of Avidin in cartilage, we used several approaches to estimate the effective net charge of the Avidin tetramer responsible for the experimental observations presented. First, the amino acid structure of Avidin suggests a net tetrameric charge of +20 based on the net excess of basic over acidic residues (see Supplementary Section S2). However, this estimate assumes that all such residues are ionized in aqueous solution and that none of these residues are internal (buried) and thereby inaccessible to charge-charge interactions within the cartilage matrix. Furthermore, this estimate neglects the effects of Avidin glycosylation which could add additional negative charge groups to the total sum. Therefore, we also applied Donnan

equilibrium theory to the experimental results of Figs. 5B and 6 to calculate Avidin charge (Supplementary Section S3). Donnan theory [53] is based on the assumptions that (1) all freely moving charged species (i.e., Avidin and bath ions) will partition into a charged tissue according to Boltzmann statistics and, (2) the net charge in the tissue is zero by electroneutrality (i.e., the sum of the tissue fixed charge density and mobile carrier concentrations). By fitting the Donnan theory to the equilibrium uptake data of Fig. 5A, the effective net charge of Avidin was calculated to be +6.2. This value is very close to the effective charge of +7.3 that we obtained by using the reported zeta potential of Avidin [54] in the Grahame equation for spherical particle electrokinetics (Supplementary Section S.4). A final upper estimate of effective net charge was obtained by assuming that the uptake of Avidin in the experiments of Figure 6 was entirely due to Donnan partitioning into cartilage in the complete absence of binding to intra-tissue sites (see Supplementary Section S.5). This estimate gave a net charge of +13 to +14.

The loss of the negatively charged GAGs soon after a joint injury might limit the extent of electrostatic interactions available for binding and retention of cationic solutes within the tissue. We simulated such a post-injury condition using chondroitinase-ABC to remove ~40% of explant GAG chains. Avidin uptake was not as high as in normal cartilage, but still achieved a very high value of 24 (Fig. 5A), and remained bound to intra-tissue sites even when placed in 1X PBS desorption bath. Together, these observations suggest that Avidin may be useful in-vivo as a model drug delivery mechanism for cartilage, and that therapeutic drug carriers with properties similar to Avidin (~7nm diameter and a high positive charge) might enable rapid, high uptake inside the cartilage, bind within the tissue, and thereby providing sustained local drug delivery.

5. Conclusion

Based on our results, we propose a mechanism for nanoparticle based drug delivery into cartilage involving highly positively charged drug carrying particles with diameter < 10 nm, which can diffuse through the full thickness of cartilage and are capable of binding to sites within the ECM. Avidin provides an excellent example of such a nanoparticle, which could potentially release and deliver low molecular weight functionalized drugs. A second approach could utilize slightly larger sized particles that can bind within the superficial zone of cartilage and then release functionalized drugs. The QD data of Fig. 3 exemplifies this approach. As these particles gradually degrade, they could release drugs which could then diffuse and/or bind to sites within the cartilage over time. With both approaches, electrostatic interactions between positively charged nanoparticles and the negative fixed charge of cartilage ECM can be optimized to augment transport, uptake and intra-tissue binding of such drug carriers.

Supplementary Material

Refer to Web version on PubMed Central for supplementary material.

Acknowledgments

This work was funded by the Deshpande Center. The authors thank Mark Belanger (Edgerton Workshop, MIT) and Dr. Shaoyan Chu (Materials Science and Engineering, MIT) for providing access and training to their manufacturing and ICP equipment, respectively. We thank Prof. Rohit Karnik (Mechanical Engineering, MIT) for his technical guidance and feedback and Hee-Sun (Bawendi Lab) for providing the Red QDs.

References

1. Le Graverand-Gastineau M-PH. Disease modifying osteoarthritis drugs: facing development challenges and choosing molecular targets. Curr Drug Targets. 2010; (5):528–35. [PubMed: 20199396]
2. Felson DT, Neogi T. Osteoarthritis: is it a disease of cartilage or of bone? Arthritis Rheum. 2004; 50(2):341–4. [PubMed: 14872473]
3. Wieland HA, Michaelis M, Kirschbaum BJ, Rudolphi KA. Osteoarthritis - an untreatable disease? Nat Rev Drug Discov. 2005; 4(4):331–44. [PubMed: 15803196]
4. Bay-Jensen A-C, Hoegh-Madsen S, Dam E, Henriksen K, Sondergaard BC, Pastoureau P, et al. Which elements are involved in reversible and irreversible cartilage degradation in osteoarthritis? Rheumatol Int. 2010; 30(4):435–42. [PubMed: 19816688]
5. Brown TD, Johnston RC, Saltzman CL, Marsh JL, Buckwalter JA. Posttraumatic Osteoarthritis: A First Estimate of Incidence, Prevalence, and Burden of Disease. Journal of Orthopaedic Trauma. 2006; 20(10):739–44. [PubMed: 17106388]
6. Anderson DD, Chubinskaya S, Guilak F, Martin JA, Oegema TR, Olson SA, et al. Post-traumatic osteoarthritis: improved understanding and opportunities for early intervention. J Orthop Res Off Publ Orthop Res Soc. 2011 Jun; 29(6):802–9.
7. Lohmander LS, Englund PM, Dahl LL, Roos EM. The long-term consequence of anterior cruciate ligament and meniscus injuries: osteoarthritis. Am J Sports Med. 2007; 35(10):1756–69. [PubMed: 17761605]
8. Irie K, Uchiyama E, Iwaso H. Intraarticular inflammatory cytokines in acute anterior cruciate ligament injured knee. Knee. 2003 Mar; 10(1):93–6. [PubMed: 12649034]
9. Kapoor M, Martel-Pelletier J, Lajeunesse D, Pelletier J-P, Fahmi H. Role of proinflammatory cytokines in the pathophysiology of osteoarthritis. Nat Rev Rheumatol. 2010 Nov 30; 7(1):33–42. [PubMed: 21119608]
10. Aaltonen KJ, Virkki LM, Malmivaara A, Konttinen YT, Nordström DC, Blom M. Systematic Review and Meta-Analysis of the Efficacy and Safety of Existing TNF Blocking Agents in Treatment of Rheumatoid Arthritis. PLoS ONE. 2012; 7(1):e30275. [PubMed: 22272322]
11. Hunter DJ. Pharmacologic therapy for osteoarthritis--the era of disease modification. Nat Rev Rheumatol. 2011; 7(1):13–22. [PubMed: 21079644]
12. Matthews GL, Hunter DJ. Emerging drugs for osteoarthritis. Expert Opin Emerg Drugs. 2011; 16(3):479–91. [PubMed: 21542666]
13. Hunter DJ. Pharmacologic therapy for osteoarthritis--the era of disease modification. Nat Rev Rheumatol. 2011; 7(1):13–22. [PubMed: 21079644]
14. Lu YC, Evans CH, Grodzinsky AJ. Effects of short-term glucocorticoid treatment on changes in cartilage matrix degradation and chondrocyte gene expression induced by mechanical injury and inflammatory cytokines. Arthritis Research & Therapy. 2011; 13(5):R142. [PubMed: 21888631]
15. Nixon AJ, Brower-Toland BD, Bent SJ, Saxer RA, Wilke MJ, Robbins PD, et al. Insulinlike growth factor-I gene therapy applications for cartilage repair. Clin Orthop Relat Res. 2000; (379 Suppl):S201–213. [PubMed: 11039770]
16. Miller RE, Grodzinsky AJ, Cummings K, Plaas AHK, Cole AA, Lee RT, et al. Intraarticular injection of heparin-binding insulin-like growth factor 1 sustains delivery of insulin-like growth factor 1 to cartilage through binding to chondroitin sulfate. Arthritis Rheum. 2010; 62(12):3686–94. [PubMed: 20722014]
17. Gerwin N, Hops C, Lucke A. Intraarticular drug delivery in osteoarthritis. Adv Drug Deliv Rev. 2006; 58(2):226–42. [PubMed: 16574267]
18. Gardner CR. Potential and limitations of drug targeting: An overview. Biomaterials. 1985; 6(3): 153–60. [PubMed: 3890975]
19. Rothenfluh DA, Bermudez H, O'Neil CP, Hubbell JA. Biofunctional polymer nanoparticles for intra-articular targeting and retention in cartilage. Nat Mater. 2008; 7(3):248–54. [PubMed: 18246072]

20. Butoescu N, Seemayer CA, Foti M, Jordan O, Doelker E. Dexamethasone-containing PLGA superparamagnetic microparticles as carriers for the local treatment of arthritis. Biomaterials. 2009; 30(9):1772–80. [PubMed: 19135244]
21. Horisawa E, Kubota K, Tuboi I, Sato K, Yamamoto H, Takeuchi H, et al. Size-dependency of DL-lactide/glycolide copolymer particulates for intra-articular delivery system on phagocytosis in rat synovium. Pharm Res. 2002; 19(2):132–9. [PubMed: 11883639]
22. Tunçay M, Cali3 S, Ka3 HS, Ercan MT, Peksoy I, Hincal AA. In vitro and in vivo evaluation of diclofenac sodium loaded albumin microspheres. J Microencapsul. 2000; 17(2):145–55. [PubMed: 10738690]
23. Vemula PK, Boilard E, Syed A, Campbell NR, Muluneh M, Weitz DA, et al. On-demand drug delivery from self-assembled nanofibrous gels: a new approach for treatment of proteolytic disease. J Biomed Mater Res A. 2011; 97(2):103–10. [PubMed: 21404422]
24. Burt HM, Tsallas A, Gilchrist S, Liang LS. Intra-articular drug delivery systems: overcoming the shortcomings of joint disease therapy. Expert Opinion on Drug Delivery. 2009; 6(1):17–26. [PubMed: 19236205]
25. Elsaid KA, Ferreira L, Truong T, Liang A, Machan J, D'Souza GG. Pharmaceutical nanocarrier association with chondrocytes and cartilage explants: influence of surface modification and extracellular matrix depletion. Osteoarthr Cartil. 2013; 21(2):377–84. [PubMed: 23186944]
26. Comper, WD. Cartilage: Molecular Aspects. Hall, BK.; Newman, SA., editors. Boston: CRC Press; 1991. p. 59-96.
27. Ng L, Grodzinsky AJ, Patwari P, Sandy J, Plaas A, Ortiz C. Individual cartilage aggrecan macromolecules and their constituent glycosaminoglycans visualized via atomic force microscopy. J Struct Biol. 2003; 143(3):242–57. [PubMed: 14572479]
28. Maroudas A. Transport of solutes through cartilage: permeability to large molecules. J Anat. 1976; 122(Pt 2):335–47. [PubMed: 1002608]
29. Snowden JM, Maroudas A. The distribution of serum albumin in human normal and degenerate articular cartilage. Biochim Biophys Acta. 1976; 428(3):726–40. [PubMed: 1276178]
30. Byun S, Sinskey YL, Lu YCS, Ort T, Kavalkovich K, Sivakumar P, et al. Transport of anti-IL-6 antigen binding fragments into cartilage and the effects of injury. Arch Biochem Biophys. 2013; 532(1):15–22. [PubMed: 23333631]
31. Garcia AM, Szasz N, Trippel SB, Morales TI, Grodzinsky AJ, Frank EH. Transport and binding of insulin-like growth factor I through articular cartilage. Arch Biochem Biophys. 2003; 415(1):69–79. [PubMed: 12801514]
32. Yao Z, Zhang M, Sakahara H, Saga T, Arano Y, Konishi J. Avidin targeting of intraperitoneal tumor xenografts. J Natl Cancer Inst. 1998; 90(1):25–9. [PubMed: 9428779]
33. Patwari P, Cook MN, DiMicco MA, Blake SM, James IE, Kumar S, et al. Proteoglycan degradation after injurious compression of bovine and human articular cartilage in vitro: interaction with exogenous cytokines. Arthritis Rheum. 2003; 48(5):1292–301. [PubMed: 12746902]
34. Liu W, Greytak AB, Lee J, Wong CR, Park J, Marshall LF, et al. Compact biocompatible quantum dots via RAFT-mediated synthesis of imidazole-based random copolymer ligand. J Am Chem Soc. 2010; 132(2):472–83. [PubMed: 20025223]
35. Wong C, Stylianopoulos T, Cui J, Martin J, Chauhan VP, Jiang W, et al. Multistage nanoparticle delivery system for deep penetration into tumor tissue. PNAS. 2011; 108(6):2426–2431. [PubMed: 21245339]
36. Liotta LA, Abe S, Robey PG, Martin GR. Preferential digestion of basement membrane collagen by an enzyme derived from a metastatic murine tumor. Proc Natl Acad Sci U S A. 1979; 76(5): 2268–72. [PubMed: 221920]
37. Farndale RW, Buttle DJ, Barrett AJ. Improved quantitation and discrimination of sulphated glycosaminoglycans by use of dimethylmethylene blue. Biochim Biophys Acta. 1986; 883(2):173–7. [PubMed: 3091074]
38. Lotz MK. New developments in osteoarthritis. Posttraumatic osteoarthritis: pathogenesis and pharmacological treatment options. Arthritis Research & Therapy. 2010; 12(3):211. [PubMed: 20602810]

39. Bendele AM. Animal models of osteoarthritis. J Musculoskelet Neuronal Interact. 2001; 1(4):363–76. [PubMed: 15758487]
40. Bonassar LJ, Frank EH, Murray JC, Paguio CG, Moore VL, Lark MW, et al. Changes in cartilage composition and physical properties due to stromelysin degradation. Arthritis Rheum. 1995; 38(2): 173–83. [PubMed: 7848307]
41. Adam C, Eckstein F, Milz S, Putz R. The distribution of cartilage thickness within the joints of the lower limb of elderly individuals. J Anat. 1998; 193(Pt 2):203–14. [PubMed: 9827636]
42. Huffman KM, Bowers JR, Dailiana Z, Huebner JL, Urbaniak JR, Kraus VB. Synovial fluid metabolites in osteonecrosis. Rheumatology (Oxford). 2007; 46(3):523–8. [PubMed: 17003168]
43. Crank, J. The mathematics of diffusion. Oxford, [Eng]: Clarendon Press; 1975.
44. Johnson DL, Urban WP Jr, Caborn DN, Vanarthos WJ, Carlson CS. Articular cartilage changes seen with magnetic resonance imaging-detected bone bruises associated with acute anterior cruciate ligament rupture. Am J Sports Med. 1998; 26(3):409–14. [PubMed: 9617404]
45. Sui Y, Lee JH, DiMicco MA, Vanderploeg EJ, Blake SM, Hung H-H, et al. Mechanical injury potentiates proteoglycan catabolism induced by interleukin-6 with soluble interleukin-6 receptor and tumor necrosis factor α in immature bovine and adult human articular cartilage. Arthritis & Rheumatism. 2009; 60(10):2985–96. [PubMed: 19790045]
46. Goldberg M, Langer R, Jia X. Nanostructured materials for applications in drug delivery and tissue engineering. Journal of Biomaterials Science, Polymer Edition. 2007; 18(3):241–68. [PubMed: 17471764]
47. Wang W, Li B, Li Y, Jiang Y, Ouyang H, Gao C. In vivo restoration of full-thickness cartilage defects by poly(lactide-co-glycolide) sponges filled with fibrin gel, bone marrow mesenchymal stem cells and DNA complexes. Biomaterials. 2010; 31(23):5953–65. [PubMed: 20488531]
48. Leddy HA, Awad HA, Guilak F. Molecular diffusion in tissue-engineered cartilage constructs: Effects of scaffold material, time, and culture conditions. Journal of Biomedical Materials Research Part B: Applied Biomaterials. 2004; 70B(2):397–406.
49. Greene GW, Zappone B, Zhao B, Söderman O, Topgaard D, Rata G, et al. Changes in pore morphology and fluid transport in compressed articular cartilage and the implications for joint lubrication. Biomaterials. 2008; 29(33):4455–62. [PubMed: 18755507]
50. Torzilli PA, Arduino JM, Gregory JD, Bansal M. Effect of proteoglycan removal on solute mobility in articular cartilage. J Biomech. 1997; 30(9):895–902. [PubMed: 9302612]
51. Torzilli PA, Grande DA, Arduino JM. Diffusive properties of immature articular cartilage. Journal of Biomedical Materials Research. 1998; 40(1):132–8. [PubMed: 9511107]
52. Byun S, Tortorella MD, Malfait A-M, Fok K, Frank EH, Grodzinsky AJ. Transport and Equilibrium Uptake of a Peptide Inhibitor of PACE4 into Articular Cartilage is Dominated by Electrostatic Interactions. Arch Biochem Biophys. 2010; 499(1–2):32–9. [PubMed: 20447377]
53. Grodzinsky, AJ. Fields, forces, and flows in biological systems. New York: Garland Science; 2011. p. 89-86.
54. Dougherty SA, Zhang D, Liang J. Fabrication of Protein Nanotubes Using Template-Assisted Electrostatic Layer-by-Layer Methods. Langmuir. 2009; 25(22):13232–7. [PubMed: 19685883]
55. Moeini M, Quinn TM. Solute adsorption to surfaces of articular cartilage explants: apparent versus actual partition coefficients. Soft Matter. 2012; 8(47):11880–8.

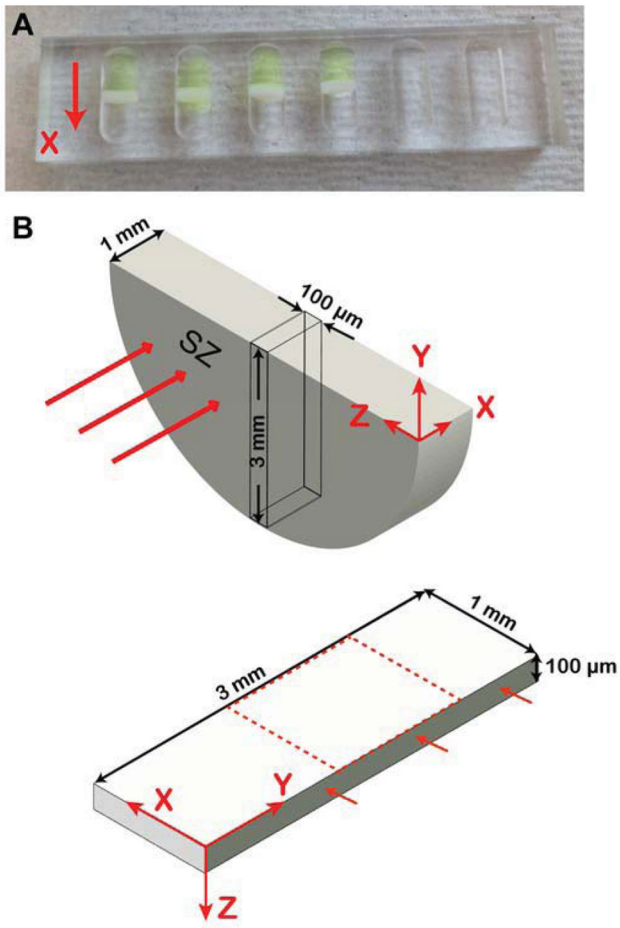

Figure 1.

(A) Transport chamber designed to enable one-way diffusion (X direction) of solutes into cartilage half disks entering from the superficial zone (**B)** A slice (100–200 μm thick) was cut from the center of the cartilage half disk (6mm diameter, 1mm thick) and imaged via confocal microscopy at 10X magnification in the X-Y plane of the slice to assess penetration and X-directed solute concentration profile after a selected duration of solute transport. Red arrows indicate the direction of solute diffusion through the superficial zone (SZ). Images of the middle region of the slice (shown by dotted boundary) were taken to avoid any edge effects from the top and bottom of the half disk. A FITC (fluorescein isothiocyanate) filter cube was used for imaging FITC conjugated solutes. Quantum dots (QDs) were imaged using a filter cube containing 565/30 nm filter for green QDs, 640/50 nm filter for red QDs and a 625 nm LP dichroic mirror.

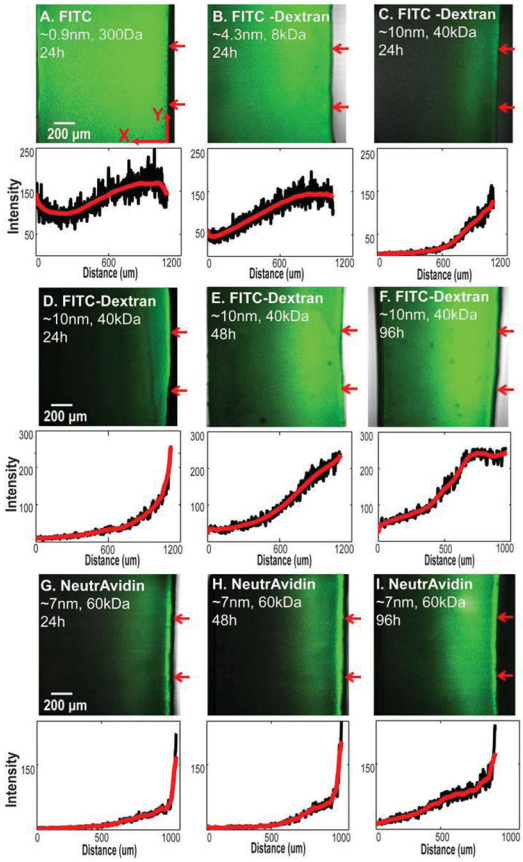

Figure 2.

Confocal images of the concentration profile inside bovine cartilage explants of **(A)** FITC (MW 389 Da, diam ~0.9 nm) **(B)** FITC-dextran (MW 8 kDa, diam ~4.3 nm) and **(C)** FITC-dextran (MW 40 kDa, diam ~10 nm) after diffusion into cartilage for 24 h. **(D)** Confocal images of the concentration profile of FITC-dextran (MW 40 kDa, diam ~10 nm) inside cartilage explants after diffusion for 24 h, **(E)** 48 h, and **(F)** 96 h. **(G)** Confocal images of the concentration profile of NeutrAvidin (neutral charge, MW 60 kDa, diam ~7 nm) after diffusion into cartilage explants for 24 h, **(H)** 48 h, and **(I)** 96 h. Arrows on the right side of the images indicate cartilage superficial zone. Average fluorescence intensities across the thickness of each slice (X direction) are plotted below the images as a function of distance from the left edge of the images. Scale bar = 200 μm.

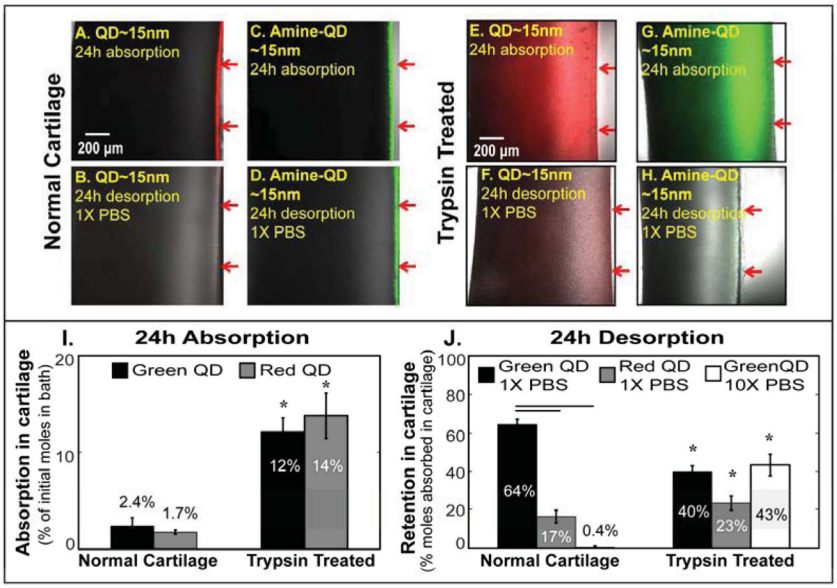

Figure 3.

Confocal images of the concentration profile inside normal cartilage explants of 15 nm in diameter, non-functionalized (RED) Cd-Se QDs after **(A)** 24 h absorption, and **(B)** 24 h desorption (into 1X PBS bath). **(C)** Confocal images of the concentration profile inside normal cartilage explants of 15 nm amine functionalized QDs (GREEN) after 24 h absorption, and **(D)** 24 h desorption (into 1X PBS bath). **(E)** Confocal images of the concentration profile of 15 nm non-functionalized QDs (RED) inside trypsin treated cartilage explants (1mg/ml, 24 h treatment) after 24 h absorption, and **(F)** 24 h desorption (into 1X PBS bath). **(G)** 24 h absorption, and **(H)** 24 h desorption (into 1X PBS bath) of amine functionalized QDs (GREEN). Arrows on the right side of the images indicate cartilage superficial zone. Scale bar = 200 μm. **(I)** The percent of the initial moles of cadmium in the bath of Cd-Se red and green QDs that were absorbed into normal and trypsin treated bovine cartilage explants in 24 h. **(J)** The percent of cadmium absorbed in 24 h that was retained inside the cartilage explants after 24 h desorption into 1X PBS for red and green QDs and into 10X PBS for green QDs only. The explants were completely digested using HNO_3, and the total cadmium was detected using inductively coupled plasma mass spectrometry (ICP-MS). Data are for both normal and trypsin treated cartilage. Values are Mean ± SEM, n= 6 cartilage samples in each condition. Horizontal lines over bars represent significant differences between treatment groups; * indicates significant difference between trypsin treated and normal cartilage; $p<0.05$.

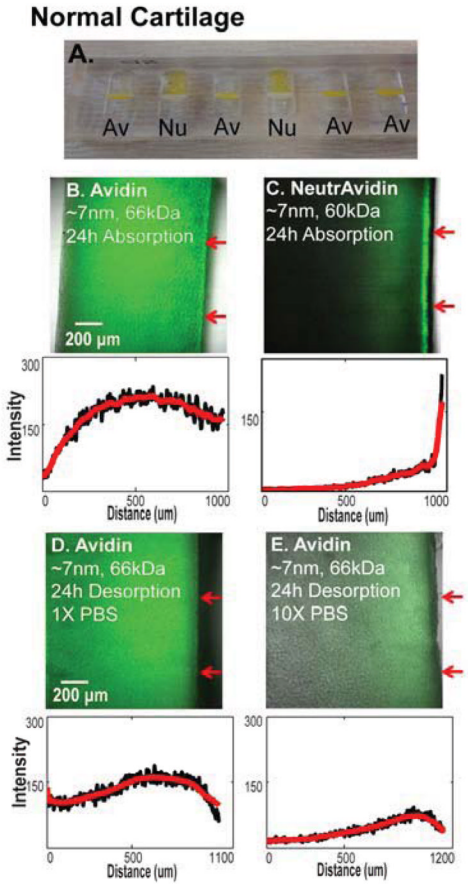

Figure 4.

(A) Transport chamber of Fig. 1A showing visual evidence of significantly higher uptake for Avidin compared to NeutrAvidin over a 24 h period. 'Av' = Avidin; 'Nu' = NeutrAvidin. **(B)** Confocal images of the concentration profile inside normal cartilage explants of Avidin (positive charge, MW 66 kDa, diam~7 nm), and **(C)** NeutrAvidin after 24 h absorption into normal cartilage explants. Confocal images after 24 h desorption of Avidin into **(D)** 1X PBS and **(E)** 10X PBS. Arrows on the right side of the images indicate cartilage superficial zone. Scale bar = 200 μm.

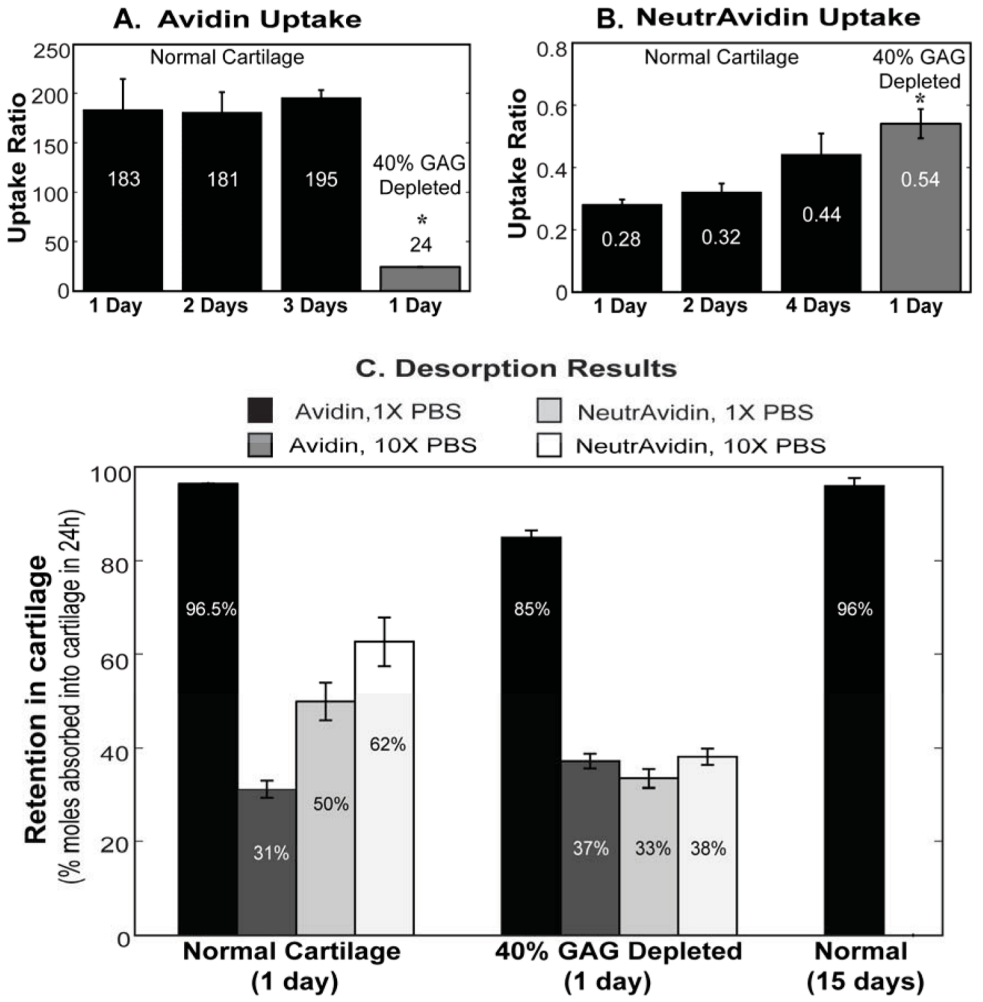

Figure 5.

Uptake ratios measured for **(A)** Avidin and **(B)** NeutrAvidin after 1 to 4 day equilibration periods for normal and 40% GAG-depleted cartilage explants (via chondroitinase-ABC) **(C)** The percent of moles absorbed in 24 h that was retained inside the explants after desorption into 1X and 10X PBS for Avidin and NeutrAvidin. Values are Mean ±SEM; n= 18 cartilage samples (6 disks from each of 3 animals) per treatment group for normal cartilage condition, and n=6 cartilage samples per treatment group (from 1 animal) for 40% GAG-depleted cartilage. Horizontal lines over bars represent statistical significant differences between treatment groups; * indicates significant difference between GAG-depleted and normal cartilage; $p<0.05$.

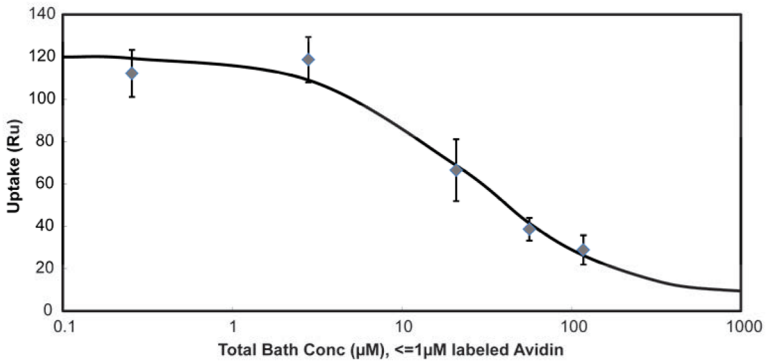

Figure 6.

Concentration dependent uptake ratio of FITC labeled Avidin in cartilage explants after 3 day equilibration at 37°C in 1X PBS supplemented with protease inhibitors. Graded amounts of unlabeled Avidin was added to a fixed amount of FITC-Avidin (<1 μM). The theoretical curve of Equation (5) (solid line) was fit to the data to obtain best-fit values of K, K_{EQ}, and N_T. The predicted values are K~6, K_{EQ}~ 150 μM and N_T~ 2920 μM. Total bath Avidin concentration is the sum of labeled and unlabeled Avidin. Data are mean ± SD, n = 4 disks per condition.

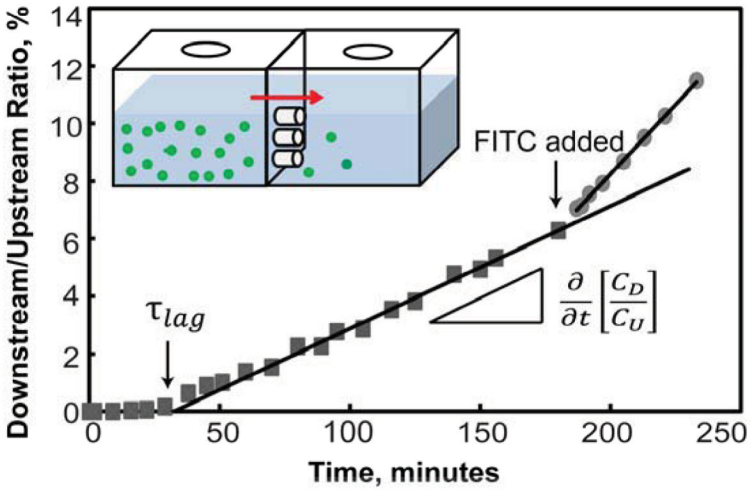

Figure 7.

Non-equilibrium diffusive transport of Avidin-FITC across a group of three 6 mm diameter, 400 μm thick cartilage explants, plotted as the measured downstream concentration versus time, normalized to the applied upstream concentration. At t = 0 min, Avidin-FITC was added to the upstream chamber. The effective diffusivity was calculated from τ_{lag} and the steady state diffusivity from the measured diffusive flux of Avidin-FITC (i.e., the slope of the concentration versus time). At t = 186 min, free FITC was added to the upstream chamber to estimate the contribution of unbound FITC to the total flux.

Table 1

Physical properties of different solute types used for diffusion studies

Solute	Average Molecular Weight (Da)	Hydrodynamic diameter (nm)	Electric Charge in solution	Molecular Structure	References
Fluorescein Isothiocyanate (FITC)	389.3	0.8–0.9	Negative	Rigid molecule	[55] Sigma Aldrich
8kDa FITC-Dextran	8000	4–4.3†	Negative	Polysaccharide, expandable coil	Sigma Aldrich
40kDa FITC-Dextran	40,000	9–10†	Negative	Polysaccharide, expandable coil	Sigma Aldrich
Avidin-FITC	66,000*	7	Positive	Globular protein; tetrameric structure; glycosylated	Invitrogen
NeutrAvidin-FITC	60,000*	7	Neutral	Globular protein; tetrameric structure; non-glycosylated	Invitrogen
Green Cd-Se Quantum Dots	X	15	Slight Positive	Spherical; Cd-Se core functionalized with amine-derivatized PEG	[34] Invitrogen
Red Cd-Se Quantum Dots	X	15	Neutral	Spherical; Cd-Se core functionalized with PEG	[34]

*MW of the tetrameric structure

†Hydrodynamic diameter in free solution when dextran is coiled [55]

Table 2

Transport properties estimated for Avidin from the transport cell and binding isotherm

Avidin Transport Properties	Binding Isotherm	Transport cell
Partitioning, K_{Avidin}	~6	~4.4
Binding density (N_T)	~2920 μM	X
Dissociation Constant (K_{EQ})	~150 μM	X
Effective Diffusivity (D_{EFF})	X	$3.8 \times 10^{-7} cm^2/s$
Steady State Diffusivity (D_{SS})	$D_{SS} = D_{EFF}\left(1 + \frac{N_T}{K_{EQ}}\right)$ $7.7 \times 10^{-6} cm^2/s$	$3.2 \times 10^{-6} cm^2/s$
Effective Charge	+6	X